Nano Technology & Nano Science Journal (NTNS)

Research Article

New Carbon Based Material Obtained By γ Quanta Irradiation With Threshold Energyof 10mev of Pure Gaseous He, Under High Pressure, In Cube2 Apparatus, Physical Properties and Aspects of New Nanotechnology

Roland Wiśniewski [1*], Gennady G. Mishinsky [3], Teresa Wilczyńska-Kitowska[2]

[1] National Centre for Nuclear Research (2004-2014), 05-400 Otwock-Świerk, Poland. Physics Faculty, Warsaw University of Technology (1952 – ret. Professor since 2000), 00-662 Warsaw, Poland.

[2]National Centre for Nuclear Research (1968 - 2014), 05-400 Otwock-Świerk, Poland.

[3]Joint Institute for Nuclear Research, Dubna, Russian Federation.

Abstract

The paper presents, observed by authors, some physical properties and possible crystallographic structure of the carbon rich (graphite-like) elements which were found in the high-pressure chamber (HPC) fulfilled before gamma irradiation only by pure gaseous helium under pressure (1 – 3) kbar. A helium HPC filled up with pure gaseous helium at initial pressure about 1.1 kbar was irradiated by braking γ-rays of 10MeV threshold energy during 1.0·105s with the electron beam current (22-24) μA. After irradiation, the residual pressure inside was much lower and equal to 430 bar. Synthesized of macroscopic amount foils of black color and of 0.22mm thickness and other multiple objects were found inside the HeHPC. The element analysis, using scanning electron microscopy (SEM) and microprobe roentgen analysis (MPRA), allowed us to establish that the foils consist predominantly of carbon and oxygen and smaller quantities of other elements (tentative weight % content: 60%C, 30%0, 3%Mg, 2% N, 0.14%Si...). Two years later some physical properties such as low density (1.20 ± 0.20 g/cm 3), high resistivity (more than E5 micro ohm m), high paramagnetic properties and medium dielectric relative constant were determined. Mechanical compressive strength to be of order of 10MPa was noted. Temperature investigation pointed out it melting temperature to be no higher than 400 0C. A new carbon-reach structure (graphite–like, with typical carbon graphite planes and with oxygen, magnesium and so on atoms between) was also postulated basing on obtained diffractometer data (using Siemens D500 powder diffractometer, equipped with high-resolution Si semiconductor detector). Also, the second method for element content determination (EDX), in principle, has confirmed the previous one. The theory of observed phenomenon was based on postulated so called trans nucleus phenomenon which took place in dense helium irradiated by proper gamma rays. Multinuclear reaction in irradiated condensed helium seems to be a new macro, micro technology.

Keywords: *Gamma Irradiation, Helium, High Pressure, Carbon, LENR.*

Introduction

The element compositions of synthesized particles and objects, as well as the surface structure of elements of the deuterium high pressure chamber (DHPC), have been studied using samples of metals such as Al, V, Cu, Pd, Sn, Re, YMn_2 alloy and stainless steel in the shape of rods and wires which were placed in molecular deuterium gas under high pressure and acted on by braking γ-rays of 10MeV [1-7] and 23MeV [8-12] energy. Analogous investigations aimed to study the possibilities of nuclear reactions were performed using hydrogen high pressure chambers (HHPC) with Pd-rods inside [13] and in the presence of hydrogen without any metallic samples in the chamber [14, 16] under irradiation by 10MeV braking γ-rays. Possible phenomenological modeling approaches for nuclear fission reactions in the liquid-drop model and for nuclear fusion are discussed in Refs. [19 - 28].

The goal of this paper is to present some interesting physical properties and possible crystallographic structure of the chosen graphite-like elements which were found in the PC fulfilled before gamma irradiation only by pure gaseous helium under pressure (1 – 3)kbar observed earlier by authors and first described in [16-18]. The mechanism of production of "foreign" chemical elements in condensed gases especially in the case of helium, basing on LENR theory, presenting in this paper is also described [29-33]. Figure 1

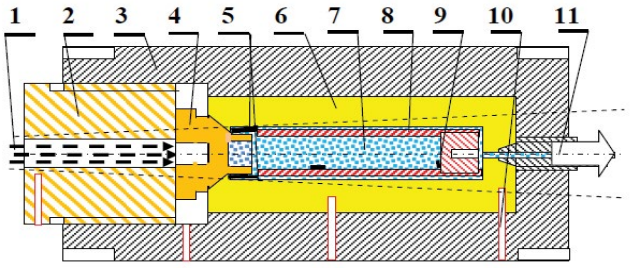

Figure 1: The schematic drawing of high pressure apparatus.1 – gamma quanta, 2 – closing screw (CuBe2), 3 – reinforcing SS high pressure chamber body, 4 - CuBe2 "window – plug" (58 °/60 ° cones), 5 – places where mainly synthesized elements were observed, 6 – CuBe2 high pressure chamber, 7 – helium under high pressure, 8 – pure Cu sleeve, 9 – expected reaction product on pure Cu plug, 10 – temperature measurement channels , 11- to high pressure valve, pressure sensor and inlet-outlet system of gaseous, < 85% of γ energy.

Corresponding author: Roland Wiśniewski, National Centre for Nuclear Research (2004-2014), 05-400 Otwock-Świerk, Poland. Physics Faculty, Warsaw University of Technology (1952 – ret. Professor since 2000), 00-662 Warsaw, Poland, Tel: 7499-196-9639; Fax: 7499-196-9639; E-mail: roland.wisniewski@gmail.com

Received: September 27, 2019**; Accepted:** October 18, 2019**; Published:** October 23, 2019.

Description of the technique

Fig. 1 shows the scheme of a modified high pressure chamber filled with helium (HeHPC) whose pressure was equal to 1092±5 bar at the start of the irradiation with γ-rays. Helium of specific spectral purification had 99.999 at.% purity specified in its data sheet. The filling of the HeHPC chamber with helium was carried out by iterations of the following operation: filling of the chamber of volume with helium up to a pressure of 0.2kbar, releasing the pressure up to atmospheric one, repeating this procedure and then filling the chamber with helium up to the 2kbar pressure. The degree of purification from atmospheric gases was approximately estimated as some ppm.

The initial pressure in the HeHPC, measured prior to irradiation using a strain sensor (see Fig.1, pos. 11) and *Model P3* measuring module, was found to be 1092bar. At helium pressure of about 1.1kbar, its atomic density is evaluated as being approximately 1.5×10^{22} at.He/cm^3 [28].

Irradiation of the HeHPC was performed during 27 hours and 51 minutes (or 1.02×10^5 s) using the MT-25 electron accelerator of the G.N. Flerov Laboratory of Nuclear Reactions of JINR, Dubna, RF. The energy of the electron beam was 10MeV, and the electron beam current ranged from 21 to 23μA. The braking γ-rays of continuous spectrums, with threshold energy of about 10MeV, were obtained using a braking target in the shape of a tungsten foil of 2.5mm thickness and an aluminum absorber of electrons with 25mm thickness. During the irradiation, the temperature inside the outer protective steel cylinder of HeHPC increased to about 60^{0}C at the steady-state regime of the chamber's irradiation. The pressure in the chamber increased at the start of irradiation from 1092bar to 1242bar, i.e. by 150bar, which seems to be a pure temperature effect. Before opening of the chamber it was the most objective and precise measurement of its inside pressure which was registered to be (426.0 ± 2.0)bar. Thus, it had dropped down by 666bar. Upon opening the chamber, a few oily (see explanation below) black foils of round shape were observed in its inside area (see Fig. 1, pos. 5).

These black foils of considerable size (see Fig. 2 below) were composed mainly of carbon. As the foils were laid out on a special clean sheet of roll paper (tracing one), it appeared that the latter (its surface) looked to be soaked with oil in the area of such foils.

After opening ~~of~~ the HeHPC chamber, foils of black color with reinforcing needles were observed at the juncture of the entrance window and reaction chamber (see Fig. 1, pos. 5), part of such needles protruding from the foils as lengthy rods of constant thickness and white color. Fig. 2 shows images of multiple black foils of round form that acquired such shape due to cylindrical symmetry of the entrance to the reaction chamber. These images were obtained using a special photo-micrographic device.

For density measurements the analytical microgram weight MYA 5.3Y Radwag, located in Microanalysis Laboratory of WUT and typical instrumentation of length and thickness measurements were used. Resistivity was measured using typical Mega ohm meter, relative dielectric constant using universal capacitance meter, and for diffraction investigations a higher standard instrumentation was used. For magnetic properties estimation a simple physical pendulum was used.

SEM and MPRA Studies of Black Thin Foils Synthesized After Irradiation γ -Rays

The structure and element composition of all the elements of the HeHPC chamber which

were in contact with dense helium, such as the cut along the cylinder symmetry axis a) two inner and outer surfaces of the beryllium bronze entrance window, b) two inside surfaces of the copper sleeve in which nuclear and chemical reactions predominantly took place, c) copper collector of reaction product, were studied at two independent analytical centers (Skobielcyn Laboratory of Moscow Łomonosow State University and FGBNU NII PMT, Moscow, Russian Federation.

As was noted in the previous section, upon opening the HeHPC, oily foils of black colour with reinforcing rods of small diameter and uniform thickness, either protruding or scattered over the surfaces of the black foils, i.e. inside them, were found at the juncture of the entrance window and reaction chamber (see Fig.1, pos. 5).

Here, results of the second Laboratory (where full elements analyses were done), will be taken under consideration. The set of foils being considered here, found after opening of the HeHPC is shown in Figure 2.

Similar to the results described by the first center, the patches of studied foil exhibit thin lengthy sticks, either observed on the foil surface or protruding in random directions. Figs 4*a* and 4*b* in [16] show SEM images of two regions of this large foil, where element content was measured. at points 18 and 19, respectively. Data shown in Table 1 give element concentrations at these two points.

Almost two and half years later, another determination of element content of investigated elements was done. Some differences were noted, such as the absence of nitrogen, smaller relative amount of oxygen and confirmation of quite large content of magnesium. See below Table 2.

Figure 2: Images of group of black foils observed at position 5, shown in Fig. 1.

Table 1: The main element composition of foils, shown in Fig. 4*a* and 4b, at two points in [16].

©	Z	weight%	at.%	weight%	at.%
		Fig. 5, p.18[16]		Fig. 5, p.19[16]	
C	6	59±7	66.38	60.7±7	67.04
N	7	5.9±1.2	5.69	5.5±1.3	5.22
O	8	30.1±3.8	25.42	32.6±4.4	27.05
F	9	-	-	0.37±0,17	0.26
Na	11	0.42±0.06	0.25	0.03±0,03	0.02
Mg	12	3.02±0.20	1.68	0.44±0,05	0.24
Al	13	0.18±0.04	0.09	0.11±0.03	0.05
Si	14	0.25±0.04	0.12	0.07±0.03	0.04

Table 2: EDX analysis of two graphite-like foils.

Element	weight%	at.%	weight%	at.%
	Point A		Point B	
C	64.31	72.00	71.43	78.36
O	30.34	25.50	23.27	19.16
Na	0.61	0.36	-	-
Mg	2.32	1.28	3.06	1.66
Al	0.08	0.04	0.08	0.04
Si	0.27	0.13	0.33	0.15
P	0.53	0.23	0.75	0.32
Cl	0.39	0.15	0.10	0.04
K	0.09	0.03	-	-
Ca	0.43	0.15	0.57	0.19
Fe	0.06	0.01	0.12	0.03
Cu	0.35	0.07	0.15	0.03
Zn	0.23	0.05	0.15	0.03

Density measurements

For this purpose two almost flat elements and regular shapes were taken under consideration. Using proper instruments the thickness was defined as (0.22 ± 0.02) mm, values of surfaces 13.3 and 20.1mm^2 with relative uncertainty ± 6% and masses 4.157 and 4.316mg. Since two values of density 1.42 and 0.98g/cm^3 and means value as a result d = (1.20 ± 0.24)g/cm^3 (relative uncertainty ±20%). Our results are related to other data for different coal phases as below see Table 3.

Resistivity Measurements

Resistivity was measured in big approximation because of non-regular form of specimen and not the best used electrical contacts. Using universal - high accuracy class - V, I, R meter we have obtained resistances of measured specimens higher than 2MΩ. Taking under consideration specimen dimensions it was possible to determine the high value of resistivity as shown in Table 3.

Magnetic Properties

The magnetic properties investigation appeared to be very interesting. Comparing behavior of diamond and investigated specimens hanging on the long diamagnetic thread during slowly coming up of the strong constant magnetic fields to the specimens it was possible to definite magnetic properties of graphite-like object. It was clear about diamagnetism of the diamond probe (no movement was observed) and para magnetism of investigated specimen (strong attraction force of investigated foils to static magnet was noted) Also a similar effect to the diamond probe was observed in pure graphite probes, its diamagnetism was observed.

Table 3: Some physical properties of different states of coal, including data for investigated probe at room temperature.

Carbon phase	Density, g/cm^3	Resistivity, μΩm	Magnetic properties
Diamond	3.47 – 3.57	10^{16} - 10^{19}	Diamagnetic
Graphite	2.10 – 2.23	//(2.5 – 5.0) and ⊥3.0 x 10^3	Diamagnetic
Amorphous state	1.8 – 2.1	(5 - 8) x 10^2	weak paramagnetism
Soot	1.6 - 2.0 (1.7-1.9)	?	weak paramagnetism
Fuleren C_{60}	1.65 - 2.6	like diamond	Diamagnetic
Graphen (0.77mg/m^2/0.5nm)	1.5	1.0 x 10^{-2}	antiferro- and ferropoints
nanotube, multiwall	0.6 – 2.0	~10	strong diamagnetic
Investigated probes	1.20 ± 0.20	>10^{10} μΩm	strong paramagnetic
C aerogels	(0.16 - 0.18) x 10^{-3}	-	-
Cu (for comparison)	8.920	1.68 x 10 $^{-2}$	Diamagnetic

Dielectric Properties

Two flat probes were covered with gold and such elements as small parallel-plate capacitors were investigated. The results are as follows – relative dielectric constant ϵr was equal to 3 – 4, what means that investigated material can belong to classical, not polar, dielectrics. Literature data for graphite ϵr = 10 – 15, for diamond ϵr = 5.5 – 10 pointed out its high values. Exemplary for: teflon 2.1, paper 3.5.

The observed difference of presented here graphite-like material relative dielectric constant relative to graphite or diamond dielectric constant is understandable because we have different materials and consequently different mechanisms of polarization.

Mechanical Properties

Preliminary studies have shown that graphite-like elements does not show homogeneous structure. The phenomenon of porosity however hasn't been noticed. They exhibit the fragility, shown in the photos, between areas of strict structure. In areas with a strict structure they also exhibit finite mechanical compression strength. In the compression probe we have noted its micro elasto-brittle state with strength 10MPa. The data, however, should be considered as indicative. No phenomenon of plasticity was observed. It also could not be established whether the investigated objects are able to loosely associate into small grains.

9. Structure of new elements of graphite-like elements XRD characterization Small part of the material called "graphite-like foils" was designed to X-ray diffraction analysis. We tried to pulverize this material in an agate crucible. The process of pulverizing has demonstrated that the material can be ground, but does not crumble as a typical inorganic material do. During shredding and grinding, parts of the material show elastic properties and cling to each other, typically as polymeric materials.

The material after this procedure was deposited on a substrate of mono crystalline silicon and analyzed with Cu Kα radiation using Siemens D500 powder diffractometer, equipped with high-resolution, Si, semiconductor detector. Registered spectrum (fig. 3) indicates a crystalline-like arrangement. The strongest line in the diffraction pattern corresponds to the distance d = 4.75Å. We are unable to identify a chemical compound on the basis of the registered diffraction pattern, as well on the basis of the largest diffraction reference data base ICDD PDF4 + 2015, but the diffraction pattern is similar to patterns of polymeric organic compounds which contain in addition to carbon and hydrogen also nitrogen, oxygen and Sulphur.

We have supposition for compose following atomic structure. We

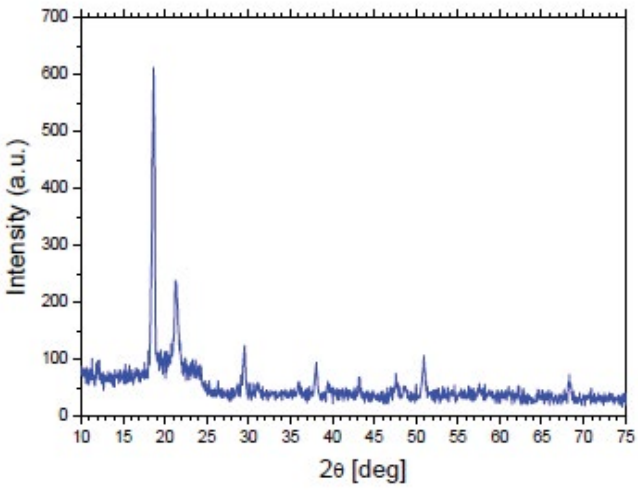

Figure 3: X-ray diffraction pattern of „graphite-like foil" sample.

have typical graphical layers and in spaces between those hexagonally ordered carbon atoms are fulfilled by - in principle - oxygen atoms and other detected by MXAP as nitrogen, magnesium and other atoms of marginal amounts. Atomic radius, valence and Van der Waalsa radiuses of C and O and N are similar. Atomic and valence radiuses of Mg are two time larger but Van der Waalsa radius is almost the same. Localization of O atoms between C layers reduces almost all free electron of carbon sp3 hybrid making element as not conducting composition.

The Structure of the Graphite-Like Objects

We propose the following, in the first step – see Figure 4, spatial phase structure graphite-like model. In this model, the position of the oxygen can be optional and have the location of the interstitial side. The position of the Mg is difficult to determine at this stage of research, even if it may be located in places like oxygen. Distance C in layers is 0.142nm, the distance between the layers of 0.475nm (0.335nm in graphite), it means of 42% larger. In Figure 5 the overview figure illustrating the existence of different forms of carbon with different densities is presented. Only the point of the diamond was set arbitrarily on the horizontal axis.

Thermal properties

The thermal properties of the graphite-like object were also an interesting problem. When we have tried to deposit on the surface of the samples the gold thin layer, in the spray chamber the temperature of investigated specimen has increased to level of (200 – 300)^{0}C. In these conditions the phenomenon of the appearance of large grains was observed, supposing melting phenomenon of the sample. (see Fig. 9). In this situation, it authors made attempts to melting phenomenon, which showed that temperature of melting of graphite-like object obtained in the process of "burning helium" is not greater than 400°C. It differs significantly from the temperatures of the fusibility of all currently known forms of carbon. The sample melted down, however, it remained non-conductive. The appearance of the sample on permanent metal (SS) ground shows photo 9. It should be noted that the sample before spraying on the background was free.

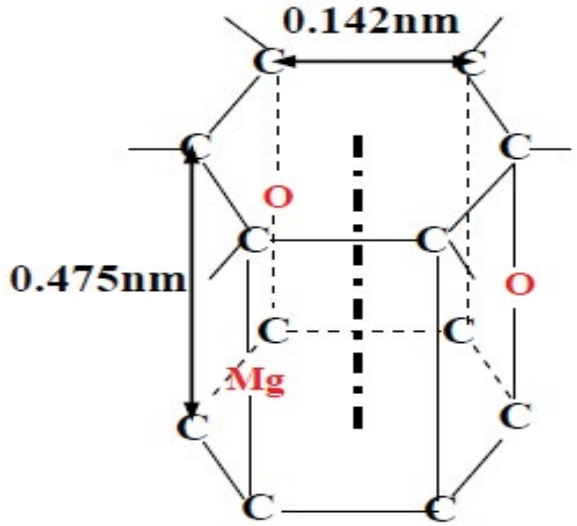

Figure 4: The first proposal of crystallographic structure for graphite-like object

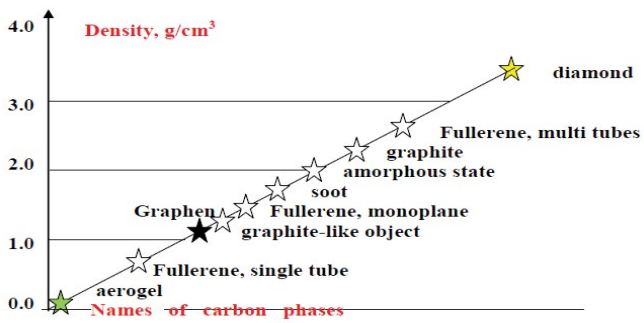

Figure 5: Illustration of known carbon phases, related to the increasing density.

Photos of Objects Being Investigated

Below few images (photos) of the described graphite-like objects, with different multiplication factor, are presented. All surfaces of objects are natural. View of photographed objects is representative for all objects found in different places in HeHPC

Investigated objects were stored in typical boxes in atmosphere typical for Laboratory Nuclear Reaction of JINR airy, without special its deactivation. In such conditions our objects were stabilized in chemical and physical senses. The color of object - typically dark does not change in any degree. Such situation is observed since 2013 so we can speak about stabilized solid state.

With physical properties testing creations graphite-like objects shows that we are dealing with a solid and crystalline object. Construction of the largest objects is like a patchwork of larger blocks. As to the formation of such macroscopic objects after several hours of the formation of specific atoms needed for their creation in the process of unknown closer to nuclear transformations is an open question. New elements are formed at the same time (different nuclear processes occurring at the same time of irradiation) Is also an interesting fact the emergence of major elements in gamma in the inlet area elements made of CuBe2 where involved in the reactions associated with kernels 9Be or short lived 8Be is possible.

Following photographs, taken on the microscope of advanced type, show more precisely the construction elements of the graphite-like objects. Common objects of dot-matrix printers are most likely dirt coming from the ground "desiccant" that come with the graphite-like object have put just after demounting of high pressure apparatus (see Figure 2). Figure 6-9 material. Manganese compound in object described here could also have an impact on the difficulties in the process of their powder spraying. For example, Allilek (sexal carbide of magnesium, solid) having crystalline structure Mg = C = C = C = Mg as well as magnesium acetylide MgC_2, (solid). Lately, using special photo-technique prof. M. Szafran and his group [29] have obtained picture suggests complicated faze structure of carbon-rich object (may be even organic compound). Figure 10

Figure 6: The photo showing natural cracks for one of investigated specimens (x200).

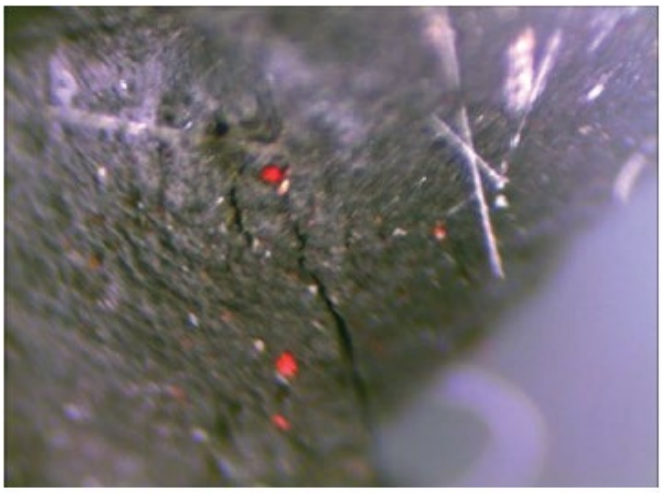

Figure 7: The photo of graphite-like object showing some colored places of not known origin (x200).

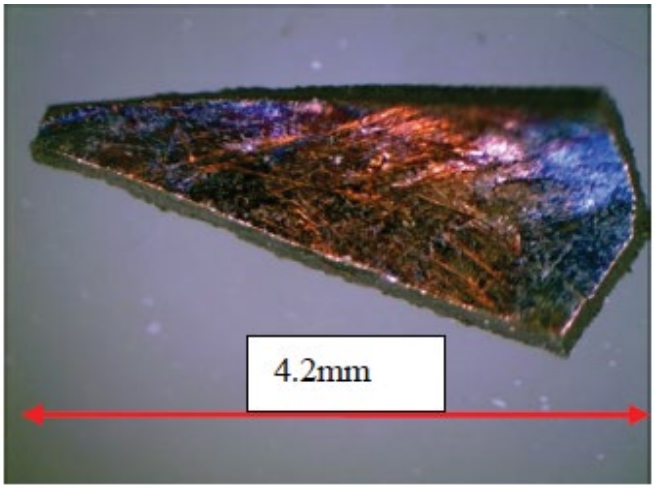

Figure 8: The photo of the gold covered surface of chosen specimen. One can see almost constant thickness of specimen! Specimen after cathode sputtering was mechanically corrected in its sides in order to avoid short circuits phenomena

Figure 9: The photo of one of two specimens after gold sputtering. Specimens have changed their look, its surface appeared a grainy structure, remaining not conductive of electrical current and closely bonded to the base material (stainless steel).

The Mechanism of Production of "Foreign" Chemical Elements in Condensed Gases

In our experiments the reactions occur at pressures of hundreds and thousands of bars. Under such pressures, the density of atoms in the gas is comparable with the density of atoms in solids or liquids. Subsequently the term condensed gas is used.

Low Energy Nuclear Reactions (LENR) occur in condensed gases upon irradiation by gamma quanta. As a result of ionization by gamma quanta of condensed matter, local regions, stable, electron-ion formations – "capsules" are formed in matter with a strong magnetic field **B** inside. "Capsules" contain a large quantity of atoms inside them. The linear size of a "capsule" is estimated at 10^{-7} cm < L < 10^{-3} cm [30]. LENR take place in those "capsules".

Both electronic and nuclear structures of atoms change in a strong magnetic field **B** inside those "capsules". Atoms, in a strong magnetic field **B** (> 30 T), inevitably turn into Transatoms and atomic nuclei in ultrastrong magnetic fields (>100 T) of transatoms are transformed into Transnuclei – Mishinsky effect [31,32]. Both the magnetic moments of the particles $\boldsymbol{\mu}$ and their orbital magnetic momentums $\boldsymbol{\mu}_\ell$ create their own magnetic fields $\mathbf{B}_\mu$ around particles, atoms and nuclei.

The transatom is an atom that has an electron Bose–Einstein condensate. The transatom electrons, not necessarily all, are in a paired state. A pair of electrons constitute an orthoboson S=1. Such pairing of two electrons occurs when the atom is in a strong magnetic field. The motion of two electrons in the orthoboson is rigidly correlated. The electron spins in the orthoboson parallel to each other $S = 1$ and both electrons are in the same energy state E(1) = E(2). It was shown in paper [31] that the pairing of electrons with parallel spins in a strong magnetic field becomes possible due to, firstly, to the exchange interaction of electrons having the character of attraction, secondly, to the appearance of correlated electron oscillations near their orbitals that generate for them a new oscillating quantum number n_b, thirdly, the sum of pulses of electrons in a pair equals to zero $\mathbf{P}_{ee} = \mathbf{0}$. The orthoboson electrons have the oscillating quantum numbers n_b and $-n_b$ (n_b=1,2,…). Therefore, the Pauli principle for them is satisfied. The trajectories of two moving paired electrons can be represented as a closed double helix (like DNA), located on the toroidal surface (Fig.11).

Since the magnetic moments of electrons in spin Bose–Einstein condensate are directed in one direction, they create a giant inhomogeneous and anisotropic magnetic field (10^5–10^{10} T) inside and around the transatom. The internal magnetic field transforms atomic nuclei into transnuclei. The external magnetic field and the electron Bose–Einstein condensate of transatoms allow them to be attracted to each other, thus creating binuclear and multinuclear molecules – transmolecules.

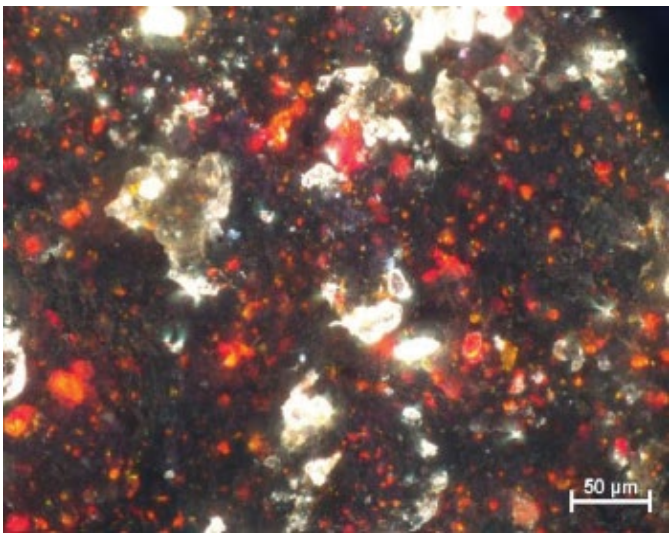

Figure 10: Photo shows a complicated phase structure of investigated specimen [29].

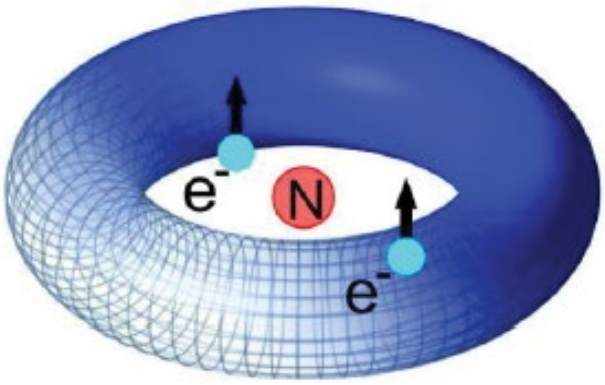

Figure 11: Orthoboson

The exchange Coulomb energy of two identical charged particles (atomic electrons, protons, atomic nuclei) paired in orthoboson has the character of attraction and it completely compensates, in the first order of perturbation theory, the energy of their Coulomb repulsion. The binding energy of paired in orthoboson electrons in a transatom increases three-fold, and the radius of their orbital decreases by three times in comparison with the binding energy and the radius of the orbital of a single electron in a multiply charged ion. Therefore, electrons in the Bose–Einstein condensate are located on the orbital closest to atomic nucleus. The wave functions of electrons in transatoms and transmolecules significantly overlap with wave functions of transnuclei. This property of transatoms and transmolecules in low energy nuclear reactions allows to overcome the prohibition on small probabilities of weak processes responsible for the transformation of protons into neutrons and vice versa.

The ultrastrong internal magnetic field of transmolecules, consisting of identical transnuclei allows the latter, due to exchange interaction, to form an orthoboson. Since the exchange energy of identical transnuclei compensates for their Coulomb repulsion, they can enter into nuclear interactions. Thus, the main prohibition on the implementation of LENR – the impossibility of passing the Coulomb barrier – is removed. Transnuclei in the transmolecule move in inhomogeneous and anisotropic space created by an ultrastrong magnetic field. Thus, motion integrals are not conserved in the interaction of the transnuclei: momentum conservation law, angular momentum (spin) conservation law, and energy conservation law are violated. As a consequence, the non-radioactive low energy nuclear reactions automatically take place in a nuclear transmolecule.

Our numerous experiments executed by A.Yu. Didyk, R. Wisniewski et al. at the FLNR of JINR demonstrate the feasibility of low energy nuclear reactions. Fig.12 shows the concentrations of elements averaged over 28 measurements in two experiments with pure hydrogen at pressures of 1 and 3.4 kbar and averaged 28 measurements in two experiments with pure helium at pressures of 1.1 and 3.05 kbar.

The most impressive result in the experiment with helium at a pressure of 1.1 kbar was the detection of thin, cylindrical, black foils of considerable dimensions in the inner part of the reaction chamber. The foils consisted predominantly of carbon. Fig.13 shows averaged concentrations of chemical elements determined by 5 measurements. A new mechanism was proposed to explain the appearance of synthesized elements in paper [33]: low energy multinuclear reactions. These reactions are caused to the creation of nuclear molecules, which consist of several helium nuclei n·^{4}He. Nuclear molecules are created by fusion of several orthohelium atoms formed as a result of ionization of helium atoms by gamma radiation followed by recombination of helium ions with electrons.

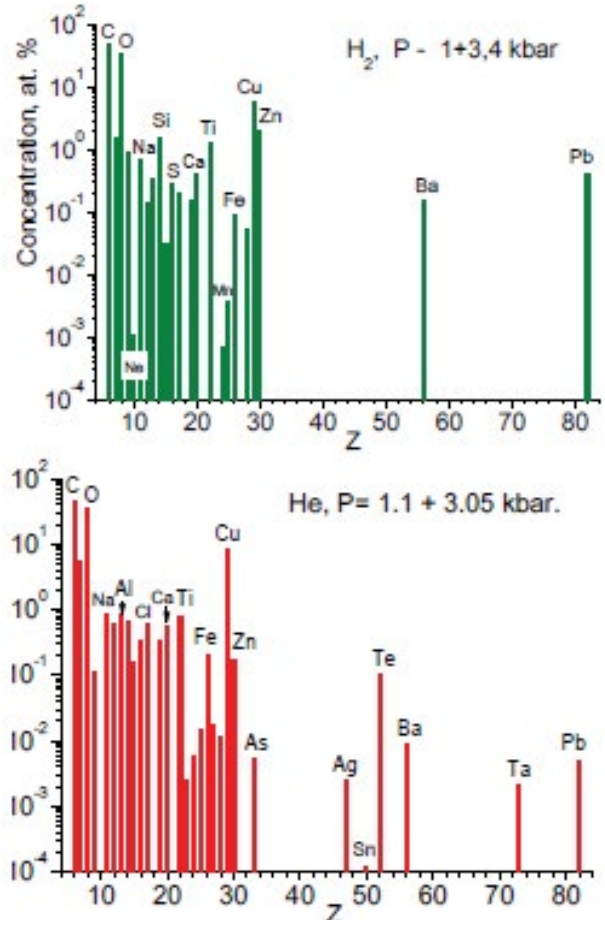

Figure 12: Elements concentration in experiments with H_2 and He.

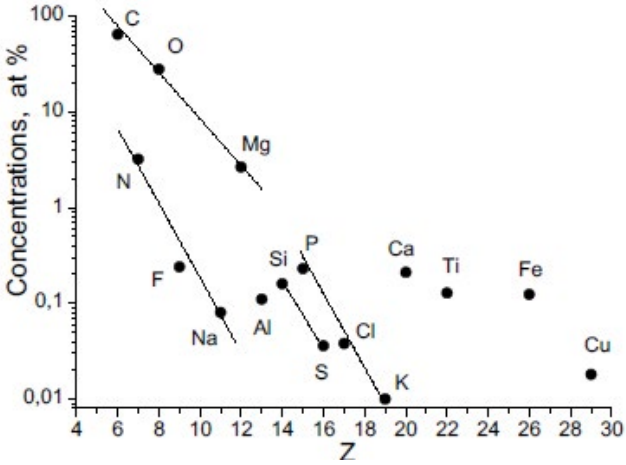

Figure 13: Averaged element concentrations by five measurements.

Orthohelium has an atomic spin $S = 1$. The radius of orbital R_1 of the first orthohelium electron is $3.1 \cdot 10^{-11}$ m, the radius of orbital R_2 of the second electron is $8.76 \cdot 10^{-11}$ m. Orthohelium, unlike parahelium, has a strong magnetic field since magnetic moments of its electrons are always parallel. The orthohelium atom has a substantial magnetic field $\mathbf{B_0}$. The calculation [34] showed that magnetic fields of orthohelium have values in the center $B_0 = 410$ *T,* and at a distance of R_2 from the center B_{R2} ~70 *T*.

We consider the interaction of two orthohelium atoms. In own a strong magnetic field, the level of the external electron 2^3S_1 splits into three levels with spin projections -1, 0, +1. The split levels will be

populated with electrons evenly. Owing to the exchange interaction orthohelium atoms with oppositely directed spins of electrons will be attracted to each other. With decreasing distance between them under the influence of Coulomb interaction, internal and external electrons begin to oscillate in them synchronously about their orbitals. Each electron acquires an additional quantum number: one is n_{1b} and the other is n_{2b}, eventually 1 and −1. Electron transitions from the split upper levels (+1, 0) to the lower level (-1) will occur under the action of an alternating magnetic field $B_R(t)$. $B_R(W(t))$ is magnetic field created by the magnetic moments of the electrons μ_e of the first orthohelium atom on electron orbitals of another orthohelium atom according to their relative velocity $W(t)$ of approaching. The electron energies become equal, but oscillating electrons remain antisymmetric. Further approaching will cause pairing of electrons and the formation of an orthoboson. The spins of orthohelium internal and external electrons are always parallel, consequently their interactions, both with electron spins of other orthohelium, and inside the atom, are always synchronous. Therefore, after the creation of electron orthobosons, the external orthoboson descends to the level of internal orthoboson. Thus, the Bose–Einstein condensate and the beryllium transmolecule "^{8}Be" are formed (Fig. 14a). The radius of transmolecule "^{8}Be" is $R_{Be} = 4.4\cdot10^{-12}$ m, and the magnetic fields: in the center B_0 (Be) = $5.4\cdot10^{5}$ T and at $1.2\cdot R_{Be}$ from the center B_R(Be) = $1.1\cdot10^{5}$ T. The atom of orthohelium in the ultrastrong alternating magnetic field of the transmolecule "^{8}Be" can be transformed into atom of the transhelium. The transhelium together with "^{8}Be" create a stable carbon transmolecule "^{12}C". It consists of three ^{4}He nuclei: two paired helium nuclei and one unpaired ^{4}He (Fig. 14b). The radius of transmolecule "^{12}C" is $R_C=3.0\cdot10^{-12}$ m, and magnetic fields: in the center of B_0(C)=$2.6\cdot10^{6}$ T and at a distance of $1.2\cdot R_C$ from the center (C)= $5.2\cdot10^{5}$ T.

Subsequently, the transmolecules "^{8}Be" and "^{12}C", due to their own ultrastrong magnetic fields, will be attracted to each other, and enter into an exchange interaction with their electron Bose–Einstein condensates. This will result in formation of multinuclear transmolecules with helium Bose–Einstein condensate. The creation of such transmolecules leads to multinuclear reactions, with the emission of protons, neutrons, alpha particles and heavy fragments (Fig.15). Green line is probability of formation n•^{4}He.) [33]:

$$n\square_2^4He \rightarrow {}_{2n-1}^{4n-1}A + p + Q\,,\; n\square_2^4He \rightarrow {}_{2n}^{4n-1}B + n + Q\,,$$

$$n\square_2^4He \rightarrow {}_{2(n-1)}^{4(n-1)}C + {}_2^4He + Q\,,\; n\square_2^4He \rightarrow A + B + C + .. + Q$$

where Q is energy released as a result of reaction.

Conclusion

Atoms of other chemical elements in the ultrastrong alternating magnetic field of the transmolecule "^{8}Be", "^{12}C" et al can be transformed into transatoms that enter into low energy nuclear reactions. In experiments with other gases: hydrogen, deuterium, xenon, as well as for helium, it should be assumed that their ionization in the condensed medium results in formation of "capsules" with a strong magnetic field inside, which leads to low energy multinuclear reactions.

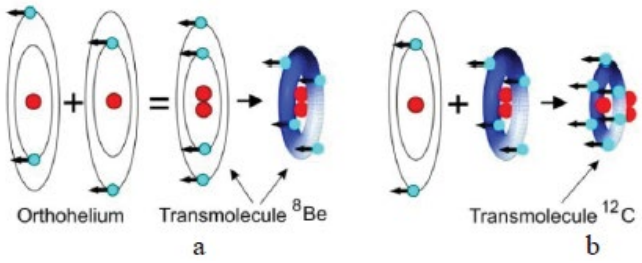

Figure 14: Formation of trans molecules ^{8}Be and ^{12}C.

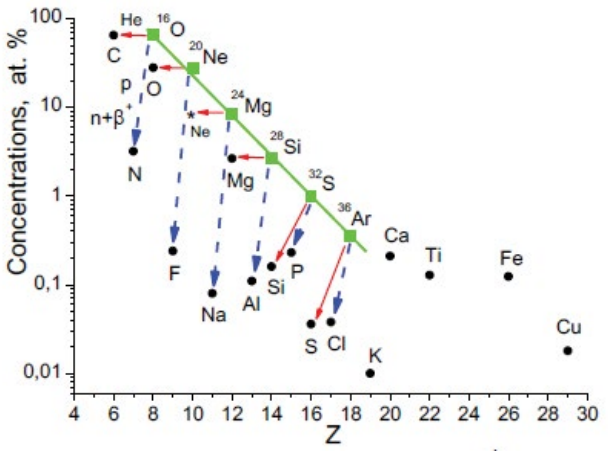

Figure 15: Transformation of trans molecules (n•^{4}He) with helium, proton or neutron emission.

A transnuclear transatom is a new state of matter: Spin-Nuclide-Electron Condensate (SNEC). The SNEC is a changed state of atomic and nuclear structure of chemical elements. The physical and chemical properties of elements change in this state. Transatoms are attracted to each other and form transmolecules with new properties that differ from those of ordinary molecules. The SNEC transnuclei can enter into nuclear reactions. A peculiarity of these nuclear reactions is the absence of irradiation during their implementation and the absence of radioactive isotopes in their products. Nuclear reactions occur after the formation of transmolecules automatically. Consequently, cross section values of nuclear reactions are comparable with cross sections values of atomic processes. Spin-nuclide-electron condensate posesses physical properties unknown up to present time. It is easy and, at the same time, difficult to predict what opportunities can be realized using these properties in science and technology. Figure 11-15 We can speak about graphite-like phase or about a quite new solid object which has been just synthesized (discovered).

During preparation of the probe to be investigated by Sherrer's powder method it was necessary to obtain its proper powder. At the beginning powdering process seems to be normal, but at the end of the process some problem seems to occur. May be some amounts of coal phase named polyynes can exist in the material Polymer character of the rest material was observed. Maybe some amount of coal phase named polyynes can exist in the material. Last obtained picture (Fig10) also suggest un normal properties of obtained objects. Also, the possibility that obtained compounds has even small organic substances in graphite-like object will have the large meaning in cosmos deliberations.

Acknowledgement

The authors thanks to dr Stanisław Gębalski, president of NSZZ (Solidarity) in NCBJ for moral help and for their interest in the subject. Thanks to Prof. Vladimir Zielevinski, (EPL editor) for his help in the process of publishing of our work, to technical specialists of the accelerator MT-25, LNR, JINR, Dubna, Russia, for cordial relations at work and commitment, dr Gennady V. Mishinsky continuator of our with A.Yu Didyk common work. Thanks to dr Piotr Konarski, dr Ryszard Diduszko from Tele Radio Technical Institute, Warsaw, Poland for element content measurements and XRD determination.

References

1. Didyk AYu, Wisniewski R, EPL (22001-6), 99 (2012).
2. Didyk AYu, Wisniewski R., EPL (42002-6), 103 (2013).
3. Didyk AYu, Wisniewski R, J. Phys. Part. Nucl. Lett. 2012. 9. No. 8. 615-631

4. Wisniewski R, Didyk AYu, Wilczynska-Kitowska T (2013) Journal of Surface Investigation. X-ray, Synchrotron and Neutron Techniques 2: 239-247.
5. Didyk AYu, Wisniewski R (2013) Inorganic Materials: Appl. Research Materials 4: 5-13.
6. Wisniewski R., Didyk AYu, Wilczynska-Kitowska T. J. Phys. Part. Nucl. Lett.
7. Didyk AYu, Wisniewski R, J. Part. Nucl. Lett. (Preprint R15-2012-63), 5 (2012), p. 22.
8. Didyk AYu, Wisniewski R, Properties of Hydrogen and Its Isotopes under High Pressure and Technological Applications. (JINR Dubna), 2013
9. Didyk AYu, Wisniewski R. JPSA 3 (4). 2013. 209-217.
10. Didyk AYu, Wisniewski R. Phys. Part. and Nucl. Lett. 2014. 11, No 2.169-179.
11. Didyk AYu, Wisniewski R. Phys. Part. and Nucl. Lett. 2014.11, No 3. 309-328.
12. Didyk AYu, Wisniewski R. Phys. Part and Nucl. Lett. 2014. 11. No. 4. 513-527
13. Didyk AYu, Wisniewski R. (part 1+2). Letters to Physics of Particles and Nuclei, 2015, 12, No. 1(192), 125-144-167;
14. Didyk AYu, Wisniewski R. Preprint R15-2014-6. Dubna. JINR. 2014. 34p.
15. Didyk AYu, Wisniewski R. J. Phys. Part. Nucl. Lett. 2013. 10. No.3 (180), 437-457;
16. Didyk AYu, Wisniewski R. and Wilczynska-Kitowska T. EPL. 2015. 109. .22001-6.
17. Wisniewski R, Didyk AYu, Wilczynska-Kitowska T. JPSA, 5(4) 2015, 268-276.
18. Wisniewski R., Wilczynska-Kitowska T and Mazarewicz P. JPSA 6(6) 2016, 1-11.
19. Ishkhanov B.S., Kapitonov I.M., IA Tutyn I.A. M.: LIBROKOM, 2009.
20. Bethe H.A. Energy Production in Stars. Phys. Rev. 1939. 55. March 1, 434-456.
21. Marshak RE, Morse PM, York H (1950) Astrophysical Journal. 111. 214-220.
22. Sierk AJ (1985) Mass-asymmetric fission of light nuclei. *Phys Rev Lett* 55: 582-583. [Crossref]
23. Oppenheimer JR, Fillips M Note for the Transmission Functions for Deuteron. Phys. Rev. 1935. 48. No.15, 500-502.
24. Shilov VM Sub-barrier fusion of spherical nuclei of medium atomic number. Nuclear Physics. 2012. 75. No. 4. 485-490.
25. Tarakanov AV, Shilov VM, Schmidt R. Nuclear Physics. 1991. 53. No. 5, 1285-1291.
26. Kálmán P, Keszthelyi T Phys.Rev. 2009. C79. 031602(R). P.031602-1-031606-4.
27. Bosch F, Faestermann T, Friese J, Heine F, Kienle P, et al. (1996) Observation of Bound-State beta - Decay of Fully Ionized 187Re: 187Re-187Os Cosmochronometry. *Phys Rev Lett* 77: 5190-5193. [Crossref]
28. Volkov VV, Cherepanov EA J. Phys. Part. Nucl. Lett. 2013. 10. No. 3: 347–353.
29. Szafran M, Wisniewski R, at al. To be published data.
30. Mishinsky GV Transatoms – Transnuclei, and their properties. The materials of the 18th Russian conference on cold transmutation of nuclei of chemical elements, 2012, Moscow, pp. 94-106 (in Russ.).
31. Mishinsky GV (2017) Atom in a strong magnetic field. Transformation of atoms to transatoms. Radioelectronics. Nanosystems. *Information Technologies (Rensit)* 9: 147-160.
32. Mishinsky GV (2018) Non-Coulomb nuclear reactions of trans atoms. Stellar energy and nucleosynthesis. *Rensit* 10: 35-52.
33. Mishinsky GV (2017) Multinuclear reactions in condensed helium. *Rensit* 9: 94-105.
34. Mishinsky GV (2017) Magnetic fields of transatoms. Spin-nuclide-electronic condensate. *International Journal of Unconventional Science* 5: 6-25.
35. Didyk AYu et al (2016) JPSA 6: 18-28.
36. Wisniewski R et al (2016) JPSA 6: 13-21.